ADVANCED OPTICAL MATERIALS
www.advopticalmat.de

Zero-Reflectance Metafilms for Optimal Plasmonic Sensing

Fumin Huang, Stacey Drakeley, Matthew G. Millyard, Antony Murphy, Richard White, Elisabetta Spigone, Jani Kivioja, and Jeremy J. Baumberg**

An ultrathin layer of metasurface that almost completely annihilates the reflection of light (>99.5%) over a wide range of incident angles (>80°) is experimentally demonstrated. Such zero-reflectance metafilms exhibit optimal performance for plasmonic sensing, since their sensitivity to changes of local refractive index is far superior to films of nonzero reflectance. Since both main detection mechanisms tracking intensity changes and wavelength shifts are improved, zero-reflectance metafilms are optimal for localized surface plasmon resonance molecular sensing. Such nanostructures have significant opportunities in many areas, including enhanced light harvesting as well as in developing high-performance molecular sensors for a wide range of chemical and biomedical applications.

1. Introduction

Metamaterials have unusual capabilities for controlling the flow of light to an extent unattained by natural materials, the well-known examples of which are negative refraction and electromagnetic cloaking.[1,2] Recently, it has been demonstrated that 2D planar metamaterials, so called metasurfaces, can significantly reduce the reflection of light, leading to nearly perfect absorption of optical energies.[3–6] Elimination of undesired specular reflection of light advances developments in many technologies, such as nonreflective lenses and displays, light harvesting in solar cells, photocatalysis, optical sensing, and molecular spectroscopy.[3,7–9] Traditionally, antireflection is achieved by impedance matching through stratified thin films.[10,11] However, this has some limitations, since in many cases it is difficult to identify exact impedance-matched natural materials, and it is also not easy to make ultrathin antireflective films with ultralow reflections (<1%).

Metamaterials provide new routes to construct ultrathin zero-reflectance films, which have many distinct advantages. Their electromagnetic properties can be custom-designed by properly engineering the nanostructures, and therefore they are no longer limited by natural materials. Conventional optical components rely on light propagation over distances much larger than the wavelength of light to shape wavefronts, accumulating phase shifts continuously during light propagation. By contrast, metasurfaces provide discontinuous abrupt changes in phase and amplitude across very short distances (much smaller than the wavelength of light). They are therefore far more efficient in shaping and controlling the flow of light,[12] enabling the development of ultrathin zero-reflectance films with thicknesses only a fraction of the wavelength of light. In addition, due to the strong light–matter interactions, metamaterials can provide extreme concentration of light, which is beneficial in many applications, such as enhancing the performance of solar cells and in molecular sensing.[3,13] For many practical applications, it is desirable to develop cost-effective ways to construct zero-reflectance metafilms in the visible range, which are insensitive to incident angle and polarization of light.

Zero-reflectance metafilms have been demonstrated in the terahertz (THz),[5] gigahertz (GHz),[6] and infrared frequency regimes,[3] with periodic structures fabricated by lithographic methods, which are difficult to scale up to meet the demands of industrial-scale applications. Alternatively, complete absorption of light in the infrared has been theoretically demonstrated to be achievable with periodically patterned graphene films.[14] Recently, Svedendahl et al. experimentally demonstrated that complete annihilation of optical reflection can be achieved with arrays of disordered Au nanodisks on glass substrates, but this was realized only within a small range of incident angles near the critical condition.[4] Here, we report that zero-reflectance metafilms in the visible range can be achieved with an ultrathin layer of metal nanoparticles, which can be simply assembled. We experimentally demonstrate that the reflectivity of a very shiny surface, such as silicon, can be completely removed with a monolayer of disordered Au nanoparticles, which are fabricated by low-cost self-assembly. The metafilms can diminish the reflection of light by more than 99.5% over a wide range of incidence (around ±40°), independent of the polarization of the incident light. The experimental results are in good agreement with simulations from an extended Maxwell–Garnett theory,

Dr. F. Huang, M. G. Millyard, Prof. J. J. Baumberg
Nanophotonics Centre
Cavendish Laboratory
University of Cambridge
Cambridge CB3 0HE, UK
E-mail: f.huang@qub.ac.uk; jjb12@cam.ac.uk
Dr. F. Huang, S. Drakeley, Dr. A. Murphy
School of Mathematics and Physics
Queen's University Belfast
Belfast, Northern Ireland BT7 1NN, UK
Dr. R. White, Dr. E. Spigone
Nokia
Broers Building
21 J J Thomson Avenue, Cambridge CB3 0FA, UK
Dr. J. Kivioja
Nokia Technologies
Karaportti 4, 02610 Espoo, Finland

DOI: 10.1002/adom.201500424

which indicate that loss plays a significant role for realizing ultrathin zero-reflectance metafilms.

We further demonstrate that such zero-reflectance metafilms are optimal plasmonic sensors. Metal nanoparticles and nanostructures are at the heart of a suite of technologies for molecular sensing. Optical properties of metal nanoparticles and nanostructures are explicitly dependent on the refractive index of surrounding medium. When molecules are adsorbed on metal nanoparticles, it invokes a change of the local refractive index and causes a shift in the optical spectra of nanoparticles, due to the localized surface plasmon resonance (LSPR).[15] This has been extensively exploited for molecular sensing in a wide range of chemical and biomedical applications, such as for the detection of proteins, pollutants, explosives, and pesticides.[15–17] Commonly there are two main detecting mechanisms for LSPR sensors. One operates at a single laser wavelength and measures the intensity changes of the reflected beam upon the adsorption of analyte molecules. Another detection mechanism measures the shift in spectral position of the plasmon resonance. Usually the main features (dips in reflection or peaks in scattering) of the optical spectra of metal nanoparticles will red shift to a longer wavelength when molecules are attached onto nanoparticles. Both detection schemes are widely implemented in LSPR sensing, with reported detection sensitivity ranging from nanomoles to attomoles.[18–20] It is of great importance to identify the plasmonic nanostructures that can produce optimal sensing performance. Here, we demonstrate that zero-reflectance metafilms are optimal plasmonic sensors with regard to both detection schemes. In both cases, their sensitivities to changes of the local refractive index of the surrounding medium are far superior to those of nonzero reflectance films. The results can be exploited for designing high-performance LSPR sensors for a wide range of applications.

2. Results and Discussion

The metafilms comprise a monolayer of spherical gold nanoparticles on silicon substrates. The Au nanoparticles (nominal diameter 150 nm, BBI Solutions) are assembled on silicon substrates with the aid of a monolayer of "glue" molecules: (3-aminopropyl)triethoxysilane (APTES) (**Figure 1**). First, silicon substrates are functionalized with a self-assembled monolayer of APTES molecules (details in the Experimental Section), and the substrates are then immersed in Au nanoparticle solutions for a time. Au nanoparticles attach to the Si substrate through the amino bonds of the APTES molecule (Figure 1a). Residual nanoparticles not binding are flushed away by rinsing the substrate in deionized water, resulting in a monolayer of nanoparticles sparsely distributed on the Si substrate. An example electron image (scanning electron microscopy (SEM)) shown in Figure 1b, clearly indicates the monodisperse distribution of nanoparticles. The density of nanoparticles can be controlled by the incubation time of the Si substrate in the nanoparticle solution. A range of samples of various nanoparticle densities are fabricated (SEM images see Figure S1, Supporting Information), with typical incubation times ranging from a few to 24 h.

Single crystal Si substrates are highly reflective, with $R = 34\%$ in the visible range. A monolayer of Au nanoparticles significantly tunes this reflectivity. **Figure 2** shows the measured reflection spectra of such nanoparticle/Si metafilms across a variety of nanoparticle densities. Starting from low nanoparticle density, the metafilm has a high reflectivity close to that of the Si substrate but modulated by plasmonic resonance effects which manifest as a distinct reflection dip around 550 nm. When the nanoparticle density increases, the dip becomes increasingly deeper until it reaches almost zero reflectance at a density of about 22 ± 2% surface coverage of nanoparticles. The dip position remains almost unchanged at low nanoparticle densities, but it then red shifts to longer wavelengths as the density of nanoparticles increases further (see solid black line tracking the dip positions). As nanoparticles get closer, interparticle coupling shifts the LSPR to longer wavelengths. The overall reflectivity across the visible range decreases as the nanoparticle density increases, which is largely due to the enhanced absorption as will be discussed later.

The reflection spectrum of the film of ≈20 ± 2% surface coverage is presented in **Figure 3**a (inset: SEM image). The reflectivity is below 5% across most regions in the visible range (400–700 nm), with a minimum reflectivity at 560 nm of 0.5%. This is a markedly low reflectivity, considering possible experimental imperfections, such as variations in nanoparticle sizes, shapes, and distributions. In fact, in ideal situations the reflectance would be perfectly zero (see below). This zero reflectance is independent of the polarization of light, when the nanoparticles are spherical shaped and randomly distributed on the Si surface. Complete optical absorption has been demonstrated on periodic patterned structures.[3,5,6,14] Here, we show that periodicity is not a necessary condition: zero-reflectance can be achieved on structures of randomly distributed nanoparticles. As disordered nanoparticle arrays can be prepared with self-assembly, this greatly reduces the fabrication cost, paving the way for large-scale applications. The response of our nanostructures is nearly omnidirectional, independent of the incident angle of light, as shown in Figure 3b. The reflectance remains almost zero up to 40° incident angle, and less than 10% up to 65° incident angle (the angular range of our goniometer).

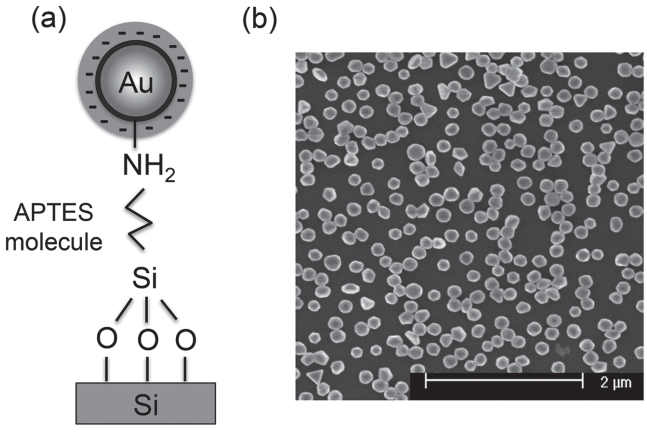

Figure 1. APTES-assisted assembly of Au nanoparticles on Si substrates. a) Schematic illustrating the attachment of Au nanoparticles onto Si through APTES molecules. b) SEM image of a sample, showing monodisperse Au nanoparticles (150 nm in diameter).

Adv. Optical Mater. 2015,
DOI: 10.1002/adom.201500424

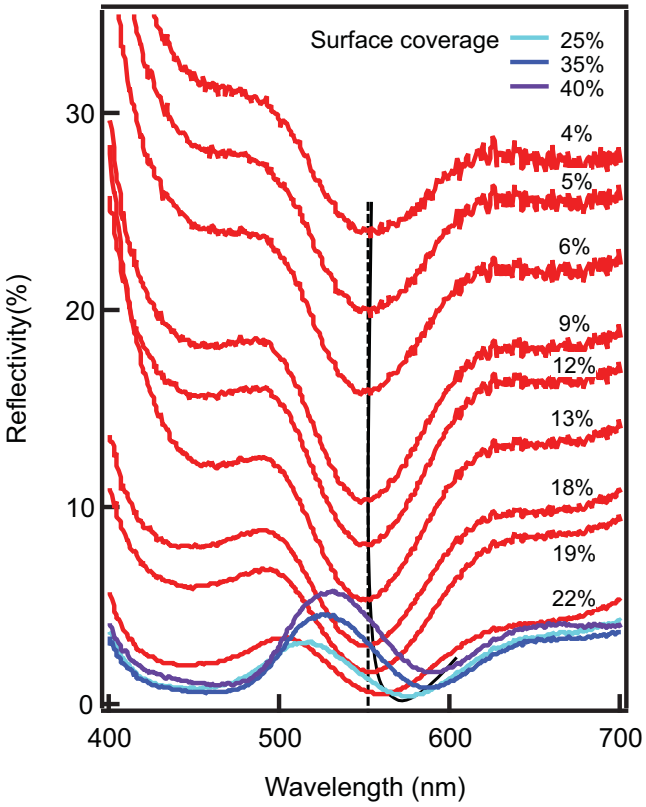

Figure 2. Measured optical reflectance spectra of a variety of Au nanoparticle metafilms on Si. From top to bottom, the surface coverage ratio (indicated by percentages. The uncertainty is about ±10%) of nanoparticles increases. For clarity, films with surface density ≥25% are shown in different colors. Black solid line indicates spectral positions of reflection dips, which red shift with increasing nanoparticle density.

As is well known, Maxwell's equations cannot be analytically solved for systems of nanoparticle arrays. An approximate solution is to treat the nanoparticle array as an effective medium, i.e., a homogeneous film with effective optical properties. This is a widely adopted method in metamaterials, such as for creating negative refractive index materials and electromagnetic cloaking devices.[1,2] Here, as a simple zeroth-order model, we use the extended Maxwell–Garnett theory to calculate the effective optical constants. For a spherical nanoparticle array, within the dipolar approximation, the effective dielectric constant is given by[21]

$$\left(\frac{\varepsilon_{\text{eff}}-\varepsilon_{\text{m}}}{\varepsilon_{\text{eff}}+2\varepsilon_{\text{m}}}\right)=\frac{\delta}{a^3}\alpha_{\text{np}} \quad (1)$$

where ε_{eff} is the effective dielectric constant of the metafilm, ε_{m} the dielectric constant of the host matrix, δ is the volume fraction occupied by nanoparticles relative to solid film, a is the radius of the spherical nanoparticles, and α_{np} is the polarizability of each nanoparticle. For small nanoparticles ($a \ll \lambda$), the polarizability can be calculated based on a quasistatic approximation, $\alpha_{\text{np}}=\frac{\varepsilon_{\text{np}}-\varepsilon_{\text{m}}}{\varepsilon_{\text{np}}+2\varepsilon_{\text{m}}}a^3$, where ε_{np} is the dielectric constant of nanoparticles.

However, nanoparticles in these experiments are not so small (150 nm in diameter) compared to the wavelength of light, hence the quasistatic approximation does not apply here. Instead, we adopt the exact Mie solution of the polarizability of a spherical particle provided by Moroz (Equation (11)) in ref. [22], which takes into account the size effects and dynamic radiation damping of the sphere.[22] By using the exact polarizability in Equation (1), we can calculate the effective dielectric constant of the nanoparticle array. The metasurface structure described above is then approximated by a thin film (with thickness 2*a*, *a* being the radius of the particle) sitting on an Si substrate (**Figure 4**a). The reflectance of such a system can be readily calculated based on classical optical theory.[23]

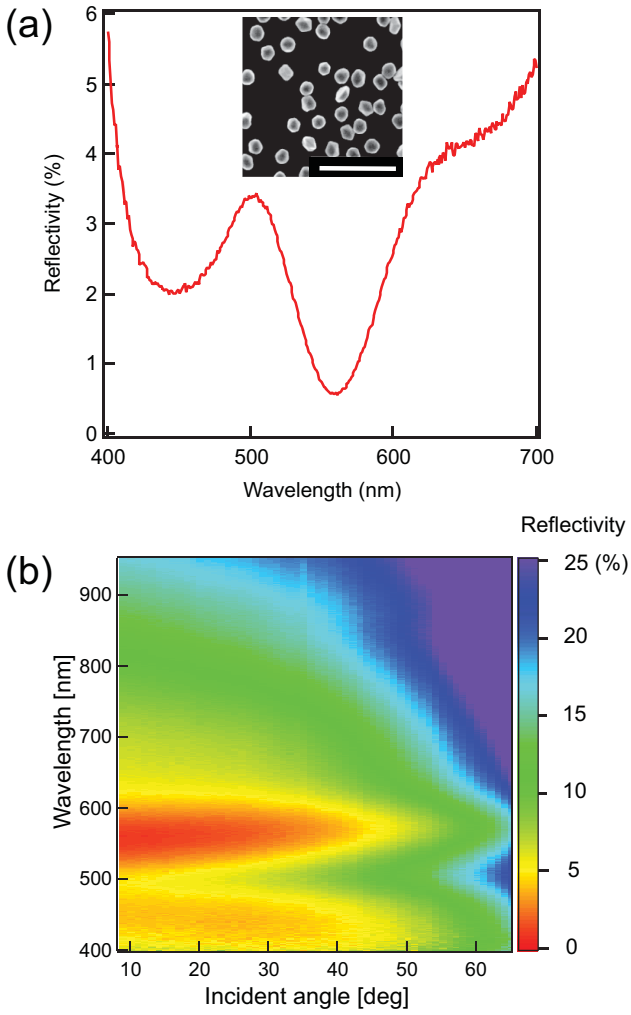

Figure 3. a) Measured reflection spectrum of a film with 20 ± 2% surface coverage, showing near zero (≈0.5%) reflection dip around 560 nm and <5% reflectivity across the whole visible range. Inset: SEM image of the nanoparticle film. Scale bar: 1 μm. b) Measured reflectance spectrum image of the above film, as a function of the incident angle of light. The near-zero reflectance is maintained up to 40° incident angle.

The resulting calculated reflectance spectra (Figure 4b) show good agreement with measured results (Figure 2). They show similar dips which deepen steadily as the nanoparticle density increases. The reflectivity reaches precisely zero at a surface coverage of ≈20%, which matches the experimental results very well. It also shows similar trends for red shift when the

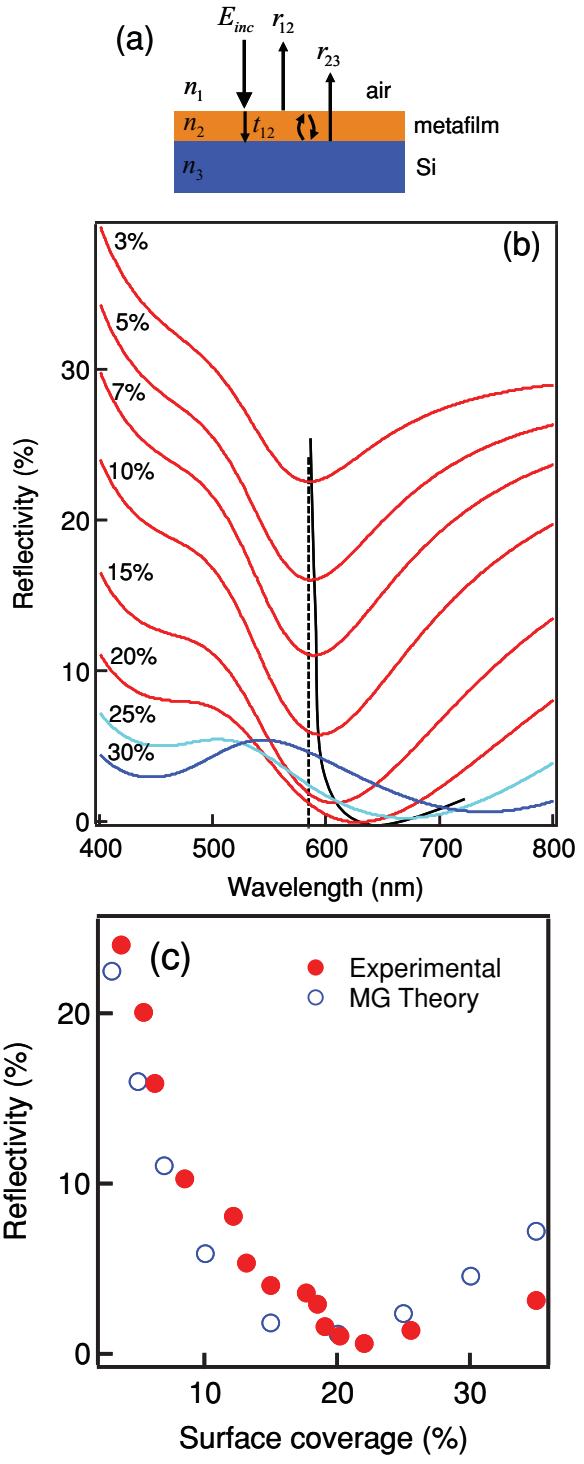

Figure 4. a) Schematic illustration of the metafilm structure. b) Calculated reflectance spectra based on Maxwell–Garnett theory. Solid black line is a guide for the spectral positions of the reflectivity minimum, which red shifts with increasing surface coverage (indicated by percentages) of nanoparticles. c) Comparison between experimental data at 550 nm (the dashed line in Figure 2) and the calculated results at 585 nm (dashed line).

nanoparticle density increases (the solid black line tracks the reflection dip position). The main discrepancy is in the exact spectral position of the reflection dip. In experimental data this is around 550 nm, whereas in simulations it is around 585 nm. This discrepancy could be caused by many factors, such as the dipole approximation adopted in the Maxwell–Garnett theory, retardation effects (as present for nanoparticles >100 nm) and the coupling between nanoparticles and the Si substrate. In Figure 4c, the experimental reflectance results measured at 550 nm (dotted line, Figure 2) are compared to the calculated results at 585 nm (dotted line, Figure 4b), and indeed agree very well for most nanoparticle arrays with modest densities (<20%). Discrepancies are larger at higher nanoparticle densities, as the dipole approximation cannot accurately account for nanoparticle coupling at close distances.

The suppression of reflection can be understood in the context of thin film interference effects. Only films of specific effective refractive index (hence nanoparticle density) are able to match the stringent phase conditions for destructive interference. However, the metasurface films are not mere destructive interference films as in conventional dielectric antireflective coatings. They provide many distinct advantages, as discussed in the following.

A single layer of Au nanoparticles can thus turn highly reflective Si substrates into a completely black surface within a narrow spectral band and significantly reduce the reflection across the whole visible range. This manifests the metasurface film distinctiveness, comprehensively controlling the flow of light at subwavelength scales. It arises from two significant factors: one is that metasurfaces produce a large phase discontinuity, and therefore are able to more effectively modulate the reflection and absorption of light in ultrathin films.[12] Another factor is that metasurface interacts strongly with light to enhance the absorption of optical energy. **Figure 5** shows the calculated effective imaginary dielectric constants of the metafilms based on the Maxwell–Garnett model described above. The spectral peak positions of the imaginary dielectric constant match those of the reflectivity dips shown in Figure 4b. The magnitude of the imaginary dielectric constant grows significantly with increasing nanoparticle density, so that enhanced optical absorption is responsible for the overall diminished reflectivity across the entire visible range (Figure 2). Loss is often considered as an obstacle in many applications of metamaterials,[24] however for the antireflection applications demonstrated here loss is advantageous for enhancing the optical absorption, making it possible to achieve zero reflectance with ultrathin (<150 nm) films.

Conventional antireflection coatings use reflective surfaces with impedance-matching dielectric films. A single layer dielectric film of quarter-wavelength thickness produces zero reflectivity at normal incidence when its refractive index matches the condition $n_2 = \sqrt{n_1 n_3}$,[23] where n_1 is the refractive index of the surrounding medium and n_3 is the refractive index of the substrate (Figure 4a). However, such ideal situations are not always achievable. For example, for glass substrates ($n_3 = 1.5$) in air ($n_1 = 1.0$), the ideal antireflective dielectric film should have a refractive index $n_2 = 1.225$, but no robust solid materials possess such a low refractive index. The closest material with suitable physical properties is magnesium fluoride (MgF_2) with a refractive index of 1.38. Glass coated with magnesium fluoride has a reflectivity of about 1% (compared to ≈4% at uncoated glass). Lower reflectivity can be achieved with multilayers of stratified thin films through interference effects, but this adds

Adv. Optical Mater. **2015**,
DOI: 10.1002/adom.201500424

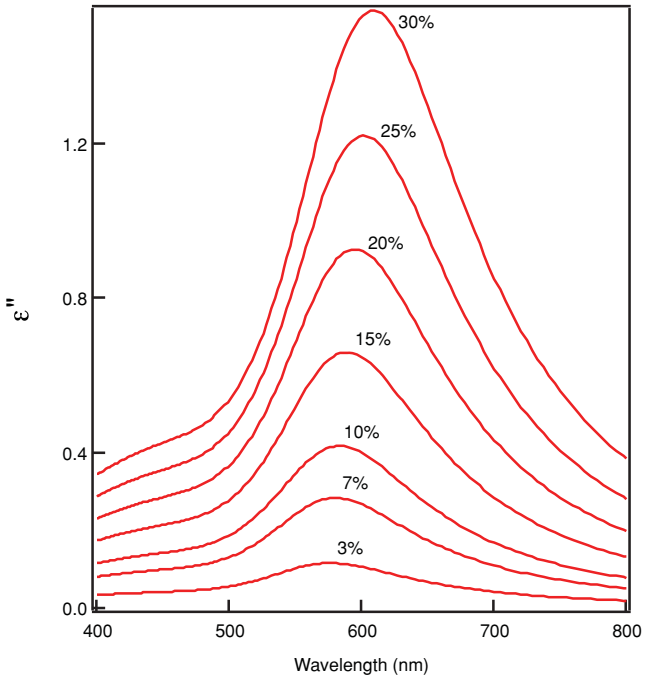

Figure 5. Calculated effective imaginary dielectric constant of the metafilms across a variety of nanoparticle densities (indicated by the surface coverage percentages).

significant cost and complexity to the fabrication, and the films have thicknesses of a few tens of wavelengths of light, only achieving minimum reflectivity at normal incidence (since the phase difference is different at different incident angles). Metamaterials as antireflection films have distinct advantages. First, they are not constrained by the optical properties of natural materials. The revolutionary paradigm of metamaterials is that their optical properties can be artificially tuned with custom-designed structures, so in principle perfect zero reflectance is achievable on any substrate. Second, they can be realized with ultrathin films over large incidence angles, as omnidirectional absorption of optical energy is possible with strong light–matter interactions.[25] Third, metamaterials have extra advantages in providing extreme concentration of light, which can enhance optical interactions in many applications, such as light harvesting in solar cells and photocatalysis. The strong reflection of Si substrates has long been a concern in solar cells, as a substantial portion of optical energy is reflected away. Depositing gold nanoparticles on Si surfaces has indeed been demonstrated to enhance the optical absorption in Si and improve photovoltaic performance significantly.[26]

The zero-reflectance metafilms are also excellent plasmonic sensors. Optical properties of the metasurface structures are highly sensitive to the local surrounding medium. Immersing the sample in water changes its color drastically (top panel, **Figure 6**a). The sample is purple in air, but appears teal in water, which can be directly distinguished by the naked eye. The reflection spectrum shifts considerably to a longer wavelength when the sample is immersed in water (Figure 6a). As mentioned above, two main detecting schemes are widely adopted in plasmonic sensing: changes of the reflectivity (∂R) or spectral shifts ($\partial\lambda$) of the reflectivity dip position (as indicated in

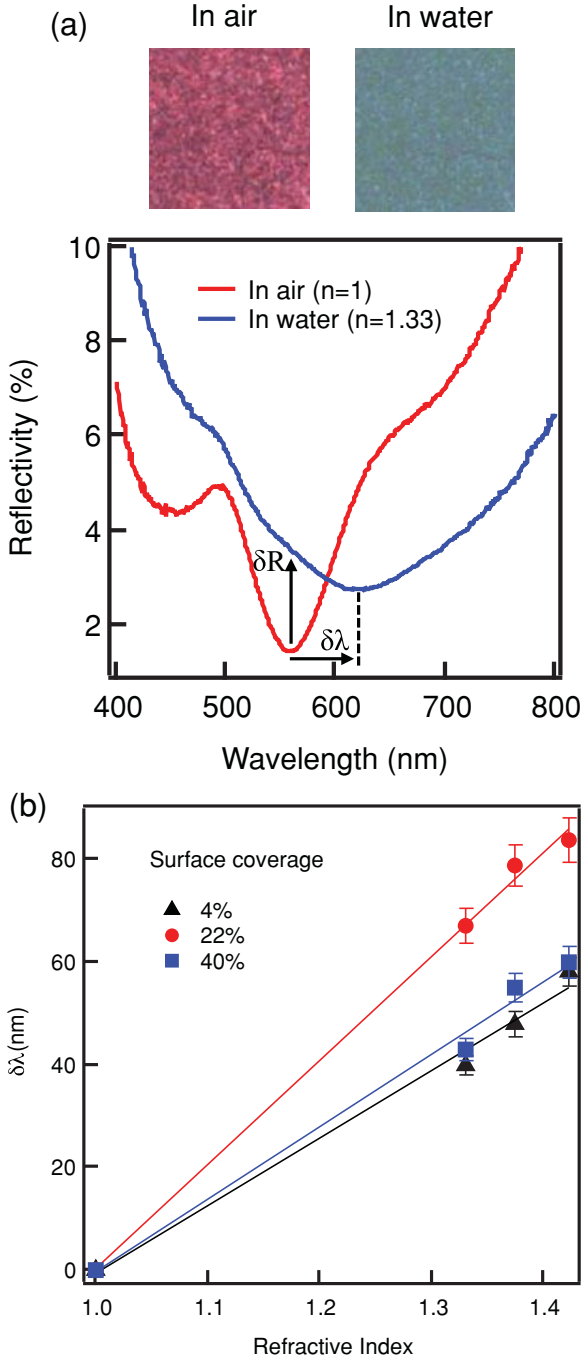

Figure 6. a) Measured optical reflectivity spectra of a metasurface sample (surface coverage ≈22 ± 2%) in air and in water, respectively. Top panel: optical images of the sample in air and immersed in water. b) Spectral shift of the reflectivity dip ($\delta\lambda$) as a function of the refractive index of surrounding media, for samples of various surface coverage. Solid lines: linear fits of the data.

Figure 6a) as a function of the refractive index. Further sensing schemes such as methods based on phase,[27,28] which also provide sensitive detection of local refractive index changes, are beyond the scope of this paper. In literature, the sensitivity of reflectivity detection schemes is defined as $S_R = \frac{1}{R(\lambda)}\frac{\partial R(\lambda)}{\partial n}|_{\lambda=\lambda_0}$,[3,29]

where R is the reflectivity, n is the refractive index, and λ_0 is the wavelength of the minimum reflectivity in air. The sensitivity of spectral shift detection is defined as $S_\lambda = \frac{\partial \lambda}{\partial n}$, which measures how much the spectral position shifts as a response to changes of local refractive index. Figure 6b shows the spectral shift ∂_λ as a function of refractive index for several metafilms of different nanoparticle densities. The spectral shift ∂_λ is linearly proportional to the refractive index, allowing sensitivities S_λ to be extracted as the gradients. We find that the sensitivity S_λ does not scale linearly with the nanoparticle density. Initially S_λ increases with increasing nanoparticle density, but after a critical nanoparticle density, it starts to decline. As shown in Figure 6b, the sensitivity of 40 ± 4% surface density films is much lower than that of films of 22 ± 2% surface density. We measured the reflection spectra of a number of samples with widely varying nanoparticle densities and systematically investigated the sensitivity of these two detection mechanisms (**Figure 7**).

To provide a clear picture of the plasmonic sensing performance of the Au nanoparticle metafilms, in Figure 7 we plot the sensitivity S_λ (red circles) and S_R (blue squares) together with the reflectivity R (black triangles) as a function of the nanoparticle density. It is evident that both sensitivities S_λ and S_R are optimal on films of minimum reflectivity, and are dramatically improved compared to low-density or high-density films. It is easy to understand why the sensitivity of S_R is optimal at zero reflectance, since from its definition it is obvious that when $R(\lambda_0) = 0$, the sensitivity S_R will be maximum. It is interesting to note that the spectral sensitivity S_λ is also maximum near the zero-reflectance, which to the best of our knowledge has not been reported before. Additional measurements with Au nanoparticles of different size (80 nm diameter) show similar results: plasmonic sensitivity S_λ is maximized on films near the minimum reflectivity (Figure S2, Supporting Information).

The above results are not only confined to films in air. Simulations based on Maxwell–Garnett theory show that the evolution of reflectivity of nanoparticle films embedded in surrounding media of different refractive indices follow a similar trend to that in air. As shown in Figure S3 (Supporting Information), the dip in reflectivity similarly deepens as the nanoparticle density increases and reaches zero reflectance on a film of 20% surface coverage (which is nearly same as that in air). However, compared to films in air, the spectral positions of the dips of films in water shift significantly to longer wavelengths, as expected since they are very sensitive to the refractive index of the surrounding medium. Simulation results show that the spectral positions of the minimum reflectivity dips are linearly dependent on the refractive index of the surrounding medium and the plasmonic sensitivity S_λ increases significantly with nanoparticle density (Figure S4, Supporting Information). The magnitudes of S_λ in simulations are larger than those observed in experiments, which is expected as the simulated reflectivity dips occur at longer wavelengths (Figure 4) where plasmonic shifts are known to be more pronounced.[30,31] In order to better compare the simulation and experimental results, the sensitivity S_λ from simulations is thus scaled down by a constant factor to match the sensitivity of the 20% surface-density film experimental results (Figure S5, Supporting Information). At low surface densities, simulations and experimental results follow similar trends. However, significant deviations appear at higher surface densities. In these simplistic simulations, the plasmonic sensitivity S_λ increases monotonically as nanoparticle density further increases, while in experiments it starts to decline after a critical nanoparticle density. This shows the limitations of the Maxwell–Garnett model (the dipole approximation can only describe the system accurately when nanoparticles are well-separated). The enhanced sensitivity at the minimum reflectivity is linked to a Fano interference effect. The dips in the reflectivity spectra (Figure 2) are well fit by Fano-resonance spectral shapes (Figure S6, Supporting Information), which originate from the coupling between the discrete plasmonic resonant spectra of nanoparticles and the continuum spectrum of Si. As Fano resonances arise from interference between two or more oscillators, they are inherently sensitive to changes of geometry or surrounding environment: small perturbations can induce dramatic changes in the lineshape or spectral shifts,[32,33] which makes Fano resonant nanostructures favorable devices for ultrasensitive molecular sensing.[33] The spectral dip in the reflectivity spectrum is an indication of an "antiresonance" behavior of the Fano resonance,[33] which is most pronounced at the minimum reflectivity, therefore exhibiting an enhanced sensitivity to the change of local environment.

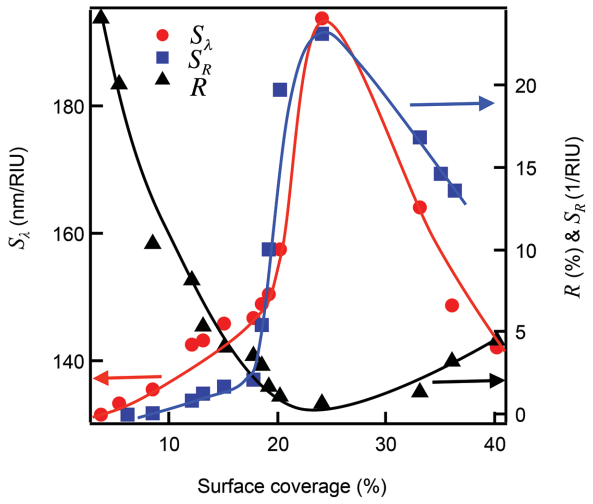

Figure 7. Plasmonic sensitivity and reflectivity as a function of the surface coverage of nanoparticles. Both the reflectivity sensitivity S_R and the spectral shift sensitivity S_λ are optimal at the minimum reflectivity. Note: the scale of S_λ refers to the left axis and those of the reflectivity R and reflectivity sensitivity S_R refer to the right axis.

LSPR sensing functionality of metal nanoparticles has been extensively studied, but so far most studies focus on the shape, size, and the chemical composition of individual nanoparticles.[16,30,31] To the best of our knowledge, it is the first time that the influence of nanoparticle density has been systematically investigated. Here we demonstrate that, for a given type of nanoparticle, optimizing the density of nanoparticle arrays can dramatically improve their plasmonic sensing performance. As shown in Figure 7, the sensitivity S_R of the zero-reflectance film is enhanced by several times compared to the low-density or high-density films, and the sensitivity S_λ is improved by about 50%. Spherical nanoparticles are normally considered to be the least favorable shape in LSPR sensing applications, as they usually

Adv. Optical Mater. **2015**,
DOI: 10.1002/adom.201500424

provide smaller plasmonic shifts compared to nanoparticles with higher aspect ratios, such as nanorods.[16] However, the optimized plasmonic sensitivity of Au nanosphere arrays reaches the same level of those of Au and Ag nanorods. The maximum reflectivity sensitivity S_R of the Au nanosphere metafilms is about 24, which reaches similar levels to that reported from Au nanorods with optimized aspect ratios.[29] The optimal spectral shift sensitivity S_λ of our Au nanoparticle metafilms is around 190 nm RIU^{-1}, much higher than most reported results with Au nanospheres[16] and similar to experimental data on Ag nanorods with zeptomole sensitivity.[19] In practical implementations, it is not only the sensitivity that matters, but the utility and detectability are also important. For example, the detectability of the dip position depends not only on how much the position shifts but also on the width and depth of the dip. In this sense, the sample of minimum reflectivity is also superior compared to most samples of higher reflectivity, as it is narrower and deeper in this condition (see Figure S6, Supporting Information). One of the limitations of zero-reflectance films is that the overall intensity is low, so high-sensitivity photodetectors may be required for the detection of small spectral shifts. In terms of utility however, the Au nanoparticle metafilms can be readily fabricated through self-assembly, and thus offer real opportunities for developing sensitive and cost-effective biochemical sensors for widespread applications.

3. Conclusion

In summary, here we experimentally demonstrate that complete annihilation of the reflectance of a highly reflective surface can be achieved with an ultrathin layer of metafilm. With a single layer of monodisperse Au nanoparticles, the reflectance of Si substrates is nearly completely annihilated (>99.5%) within a narrow band in the visible range, and significantly diminished (>95%) across the whole visible range (400–700 nm). Such zero-reflectance metafilms are insensitive to the polarization and the incident angle (around ±40°) of light, and can be fabricated by cost-effective self-assembly, therefore providing new routes to construct ultrathin antireflection films with potential applications in many areas. Furthermore, we demonstrate that the zero-reflectance metafilms are optimal plasmonic sensors. Their sensitivity to the local refractive index is greatly superior to that of nonzero reflectance films (for films composed of same nanoparticles), in both the two main detection mechanisms of LSPR sensors. Although these results are demonstrated with spherical Au nanoparticles, these general principles should be applicable to other nanoparticles and metamaterial structures. By tuning the working frequency to the spectral position of zero reflectivity or engineering the structures to be zero-reflectance films, the sensitivity of many existing and future LSPR sensors will be significantly improved, which will have significant implications for developing high-performance molecular sensors.

4. Experimental Section

APTES Self-Assembly: APTES molecules were diluted in toluene with a volume ratio of 1:100 (APTES:toluene). Si substrates were pretreated by rinsing with acetone, heptane, and isopropanol solvents in successive order, and blown dry with N_2 gas, after which they were then immersed in APTES solution (which was preheated to 70 °C in a glass dish). After ≈1 h, substrates were taken out and rinsed first with toluene to remove excess APTES molecules and then rinsed with deionized water and dried with N_2 gas.

Refractive Index Sensing: A range of liquids of various refractive indices were prepared by mixing deionized water with glycerol at different ratios. This produces solutions with refractive indices ranging from 1.33 (water) to 1.47 (glycerol).

Optical Spectroscopy: Optical reflectivity spectra (Figure 2) were measured on a modified optical microscope (Olympus, BX51). Unpolarized incandescent white light was used to illuminate samples through a 10× objective (NA 0.25) from above. The reflected light was collected by the same objective and coupled to a spectrometer (QE65 Pro, Ocean Optics) through a multimode optical fiber. The image of the angle-dependent reflectivity (Figure 3) was measured on a home-built goniometer setup, with collimated beams incident from various angles (from 10° to 65°) and the reflected beams were collected and coupled to a spectrometer (QE 65000, Ocean Optics).

Supporting Information

Supporting Information is available from the Wiley Online Library or from the author.

Acknowledgements

The authors would like to thank Nokia Research Centre (Cambridge), EPSRC grant EP/G060649/1, and ERC LINASS 320503 for financial support.

Received: July 30, 2015
Revised: October 7, 2015
Published online:

[1] J. B. Pendry, A. J. Holden, W. J. Stewart, I. Youngs, *Phys. Rev. Lett.* **1996**, *76*, 4773.
[2] D. Schurig, J. J. Mock, B. J. Justice, S. A. Cummer, J. B. Pemdry, A. F. Starr, D. R. Smith, *Science* **2006**, *314*, 977.
[3] N. Liu, M. Mesch, T. Weiss, M. Hentschel, H. Giessen, *Nano Lett.* **2010**, *10*, 2342.
[4] M. Svedendahl, P. Johansson, M. Kall, *Nano Lett.* **2013**, *13*, 3053.
[5] C. M. Watts, X. Liu, W. J. Padilla, *Adv. Mater.* **2012**, *24*, OP98.
[6] Y. Yao, R. Shankar, M. A. Kats, Y. Song, J. Kong, M. Loncar, F. Capasso, *Nano Lett.* **2014**, *14*, 6526.
[7] J. Zhu, Z. Yu, G. F. Burkhard, C.-M. Hsu, S. T. Connor, Y. Xu, Q. Wang, M. McGeheee, S. Fan, Y. Cui, *Nano Lett.* **2009**, *9*, 279.
[8] L. Li, T. Hutter, A. S. Finnmore, F. M. Huang, J. J. Baumberg, S. R. Elliott, U. Steiner, S. Mahajan, *Nano Lett.* **2012**, *12*, 4242.
[9] F. M. Huang, D. Wilding, J. D. Speed, A. E. Russell, P. N. Bartlett, J. J. Baumberg, *Nano Lett.* **2011**, *11*, 1221.
[10] G. Hass, H. H. Schroeder, A. F. Turner, *J. Opt. Soc. A* **1956**, *46*, 31.
[11] I. Moreno, J. J. Araiza, M. A-Alejo, *Opt. Lett.* **2005**, *30*, 914.
[12] N. Yu, P. Genevet, M. A. Kats, F. Aieta, J.-P. Tetienne, F. Capasso, Z. Gaburro, *Science* **2011**, *334*, 333.
[13] K. Aydin, V. E. Ferry, R. M. Briggs, H. A. Atwater, *Nat. Commun.* **2011**, *2*, 517.
[14] S. Thongrattanasiri, F. H. L. Koppens, F. J. Garcia de Abajo, *Phys. Rev. Lett.* **2012**, *108*, 047401.
[15] K. A. Willets, R. P. Van Duyne, *Annu. Rev. Phys. Chem.* **2007**, *58*, 267.
[16] K. M. Mayer, J. H. Hafner, *Chem. Rev.* **2011**, *111*, 3828.
[17] A. G. Brolo, *Nat. Photonics* **2012**, *6*, 709.

[18] C. Rosman, J. Prasad, A. Neiser, A. Henkel, J. Edgar, C. Sonnichsen, *Nano Lett.* **2013**, *13*, 3243.
[19] A. D. McFarland, R. P. Van Duyne, *Nano Lett.* **2003**, *3*, 1057.
[20] J. Ferreira, M. J. L. Santos, M. M. Rahman, A. G. Brolo, R. Gordon, D. Sinton, E. M. Girotto, *J. Am. Chem. Soc.* **2009**, *131*, 436.
[21] Y. Battie, A. Resano-Garcia, N. Chaoui, Y. Zhang, A. E. Naciri, *J. Chem. Phys.* **2014**, *140*, 044705.
[22] A. Moroz, *J. Opt. Soc. Am. B* **2009**, *26*, 517.
[23] M. Born, E. Wolf, *Principles of Optics*, Cambridge University Press, UK **1999**.
[24] A. Boltasseva, H. A. Atwater, *Science* **2011**, *331*, 290.
[25] T. V. Teperik, F. J. Garcia de Abajo, A. G. Borisov, M. Abdelsalam, P. N. Bartlett, Y. Sugawara, J. J. Baumberg, *Nat. Photonics* **2008**, *2*, 299.
[26] D. Wan, H.-L. Chen, T.-C. Tseng, C.-Y. Fang, Y.-S. Lai, F.-Y. Yeh, *Adv. Funct. Mater.* **2010**, *20*, 3064.
[27] V. G. Kravets , F. Schedin, R. Jalil, L. Britnell, R. V. Gorbachev, D. Ansell, B. Thackray, K. S. Novoselov, A. K. Geim, A. V. Kabashin, A. N. Grigorenko, *Nat. Mater.* **2013**, *12*, 304.
[28] M. Svedendahl, R. Verre, M. Kall, *Light: Sci. Appl.* **2014**, *3*, e220.
[29] J. Becker, A. Trugler, A. Jakab, U. Hohenester, C. Sonnichsen, *Plasmonics* **2010**, *5*, 161.
[30] K.-S. Lee, M. A. El-Sayed, *J. Phys. Chem. B* **2006**, *110*, 19220.
[31] M. M. Miller, A. A. Lazarides, *J. Phys. Chem. B* **2005**, *109*, 21556.
[32] M. Svedendahl, M. Kall, *ACS Nano* **2012**, *6*, 7533.
[33] B. Luk'yanchuk, N. I. Zheludev, S. A. Maier, N. J. Halas, P. Nordlander, H. Giessen, C. T. Chong, *Nat. Mater.* **2010**, *9*, 707.

Adv. Optical Mater. **2015**,
DOI: 10.1002/adom.201500424